



CHORUS

This is the accepted manuscript made available via CHORUS. The article has been published as:

Characterization of coherent population-trapped states in a circuit-QED Λ system

Shavindra P. Premaratne, F. C. Wellstood, and B. S. Palmer

Phys. Rev. A **96**, 043858 — Published 25 October 2017

DOI: [10.1103/PhysRevA.96.043858](https://doi.org/10.1103/PhysRevA.96.043858)

Characterization of coherent population trapped states in a circuit QED Λ -system

Shavindra P. Premaratne,^{1,2,*} F. C. Wellstood,^{1,3} and B. S. Palmer^{1,2}

¹*Department of Physics, University of Maryland, College Park, Maryland 20742, USA*

²*Laboratory for Physical Sciences, College Park, Maryland 20740, USA*

³*Joint Quantum Institute and Center for Nanophysics and Advanced Materials, College Park, Maryland 20742, USA*

We examined coherent population trapping in a circuit-QED system consisting of an Al/AIO_x/Al transmon qubit embedded in an Al 3D cavity. By engineering the dissipation rate of the cavity to be much larger than that of the qubit and continuously pumping a two-photon process to an excited state of the cavity-qubit system, we were able to invert the population into the qubit excited-state with a fidelity of 94%. Applying a second continuous drive tone at the dressed cavity frequency forms an effective Λ -system and enabled us to coherently trap the system into a dark state formed from a superposition of the excited and ground states of the qubit. By performing quantum state tomography we demonstrated that the position of the dark state on the Bloch sphere can be controlled by changing the relative amplitudes and phases of the two drives.

I. INTRODUCTION

Quantum dark states were first observed in naturally occurring physical systems that can become trapped in a state with a forbidden optical transition, preventing the absorption or emission of photons [1]. Because of their long lifetimes, dark states are potential candidates for quantum memory elements [2, 3]. Dark states can also be generated in systems with three or more levels by simultaneously driving multiple levels in the system, creating a coherent superposition state with a vanishing optical transition matrix element [4–6]. For example, pumping a three-level Λ -system (levels denoted by $|0\rangle$, $|1\rangle$ and $|2\rangle$) with one oscillatory drive field on the $|0\rangle \leftrightarrow |1\rangle$ transition and a second drive field on the $|1\rangle \leftrightarrow |2\rangle$ transition, results in the system being driven into the dark state

$$|D\rangle = \cos\Theta|0\rangle + e^{i\phi}\sin\Theta|2\rangle. \quad (1)$$

Here, the mixing angle Θ is controlled by the ratio between the two drive strengths [6], and ϕ is controlled by the phase difference between the drives [7].

Recently, Novikov *et al.* [8] described a Λ -system formed from a transmon-cavity system within a circuit-QED (cQED) architecture [9, 10]. The $|0\rangle \leftrightarrow |1\rangle$ arm of the Λ -system was driven by pumping the system from the ground state $|g0\rangle$ to state $|e1\rangle$, corresponding to both the qubit and cavity being excited. The $|1\rangle \leftrightarrow |2\rangle$ arm of the Λ -system was driven using the cavity-like transition $|e0\rangle \leftrightarrow |e1\rangle$, with the qubit in the excited state. Simultaneously driving the two arms of the Λ -system drives the composite system into a dark state $|D\rangle$ and signatures of both coherent population trapping [1, 4] and EIT [11] were demonstrated [8].

In this cQED Λ -system, the maximum fidelity for the dark state was set by the ratio of decay rates between the cavity and the qubit. This ratio was engineered to be large, to achieve high dark state fidelity. Dissipation

engineering [12, 13] has been used elsewhere with quantum superconducting devices for stabilizing single qubit states [14, 15] and entangled two qubit states [16]. Geerlings *et al.* [17] also used the large dissipation of a cavity in conjunction with a double drive to rapidly reset a qubit to a known fiducial state. Similar techniques have been used in nanomechanics to cool mechanical oscillators to their ground state [18, 19].

In this article, we use quantum state tomography [20] to examine dark states in a Λ -system similar to the one described by Novikov *et al.* [8]. In section II we describe our cQED Λ -system in detail. Section III discusses the spectroscopy of our driven Λ -system and how we determined key system parameters. Tomographic measurements of the dark state are presented in section IV. Over a broad range of values for Θ and ϕ , we find that the tomographic data is in good agreement with theory, demonstrating that the states are being generated as predicted. We conclude in section V with a discussion of the degree of state control we were able to achieve.

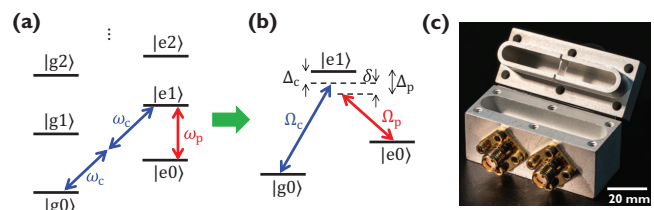


FIG. 1. (Color online) **Cavity-qubit system.** (a) Jaynes-Cummings ladders showing combined cavity-qubit energy levels. The number within a ket indicates the number of photons in the cavity while $|g\rangle$ and $|e\rangle$ represent the qubit ground and excited states, respectively. (b) Model of the cavity-qubit system as a three-level system undergoing CPT. (c) Photograph of transmon chip placed in aluminum 3D cavity.

* shavi@umd.edu

II. cQED SYSTEM

Our cQED system consisted of a transmon [21] embedded in a three-dimensional superconducting Al microwave cavity [22] that was cooled on a Leiden CF-450 dilution refrigerator with a base temperature of 20 mK. The transmon had a single Al/AlO_x/Al Josephson junction and two large Al pads which capacitively shunted the junction. The transition frequency between the ground and first excited state was $\omega_q/2\pi = 6.33121$ GHz. The energy relaxation time was $T_1 = 6.7$ μ s and the spin echo coherence time was $T_2 = 11.7$ μ s. The TE₁₀₁ fundamental mode of the cavity had a dressed resonance frequency $\omega_r/2\pi = 7.94593$ GHz and was coupled to the qubit with a strength $g/2\pi = 83$ MHz. In the limit $g \ll \Delta = \omega_r - \omega_q$, the undriven system can be described by the dispersive Jaynes-Cummings Hamiltonian [23],

$$\mathcal{H}_{JC} = \frac{1}{2}\hbar\omega_q\hat{\sigma}_z + \hbar(\omega_r - \chi\hat{\sigma}_z)\hat{N} \quad (2)$$

where the Pauli z-operator $\hat{\sigma}_z$ acts on the qubit, \hat{N} is the cavity photon number operator and $\chi/2\pi = 4.3$ MHz is the dispersive shift due to the cavity-qubit interaction.

The Jaynes-Cummings Hamiltonian leads to energy levels of the combined system that can be represented by two ladders (Fig. 1(a)), one for the qubit in the ground state $|g\rangle$ and the other for the qubit in the excited state $|e\rangle$. The separations of the rungs for the $|g\rangle$ and $|e\rangle$ ladders are $\omega_r + \chi$ and $\omega_r - \chi$ respectively. The three states used for coherent population trapping are $|g0\rangle$, $|e0\rangle$, and $|e1\rangle$ with the dark state being a superposition of $|g0\rangle$ and $|e0\rangle$ [8]. The $|g0\rangle \leftrightarrow |e1\rangle$ transition forms one arm of our Λ -system and the corresponding drive is denoted as the coupler, with amplitude Ω_c and frequency ω_c . The $|e0\rangle \leftrightarrow |e1\rangle$ transition is the second arm of the Λ -system and the corresponding drive is denoted as the probe, with amplitude Ω_p and frequency ω_p (Fig. 1(b)).

Coherent population trapping in this Λ -system requires the $|e0\rangle \rightarrow |g0\rangle$ transition to have a longer lifetime than the $|e1\rangle \rightarrow |e0\rangle$ transition. This was accomplished by adjusting the lengths of the launcher-pins which couple the cavity to the input and output microwave lines. Setting the external coupling of the cavity at room temperature to $Q_E = 3000$ gave a cavity lifetime of $\kappa^{-1} = 50$ ns at low temperatures.

III. SPECTROSCOPY

A. Population inversion via two photon transition

In addition to requiring $\kappa \gg \Gamma_1$, coherent population trapping also requires sufficiently fast Rabi pumping of the system. In particular for a continuous drive, to create significant population inversion into $|e0\rangle$, the system must be driven faster than the rate of spontaneous emission from $|e0\rangle$. For our cQED system, the $|g0\rangle \leftrightarrow |e1\rangle$

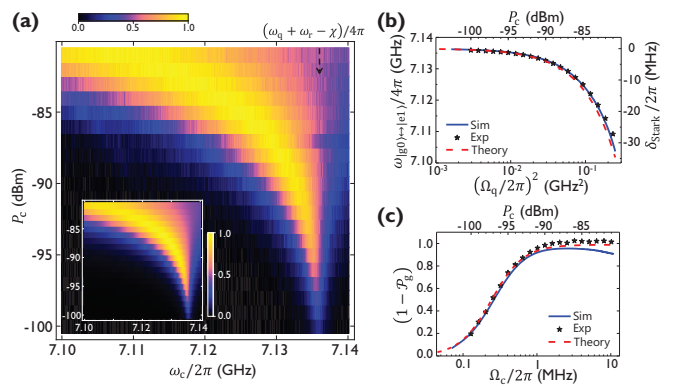


FIG. 2. (Color online) **Two-photon spectroscopy.** (a) False color plot of measured excited-state probability \mathcal{P}_e versus coupler frequency ω_c and coupler drive power P_c . (inset) Simulated false color plot from solving the master equation. (b) Measured Stark shift δ_{Stark} versus P_c (black stars) compared with the results from master equation simulations (solid blue) and analytical Eq. 4 (dashed red). (c) Maximum measured excited state probability (black stars) versus effective coupler drive strength Ω_c calculated using Eq. 3. Solid blue curve shows results from master equation simulations and the dashed red curve shows plot from Eq. 6.

transition is a second order process involving the absorption of two coupler photons and this gives a relatively small pump rate unless a relatively high power is used [24, 25]. Kindel *et al.* [26] demonstrated that a similarly engineered system utilizing this two-photon process could be used as a source of itinerant photons.

Figure 2(a) shows a false color plot of the qubit excited state population \mathcal{P}_e versus the coupler drive power P_c and coupler frequency near $(\omega_q + \omega_r - \chi)/4\pi$. The qubit state was interrogated using a Jaynes-Cummings high-power readout at the cavity bare frequency of 7.92241 GHz [27]. Above a drive power of -100 dBm, we observe a dramatic increase in the occupancy of the qubit excited state. The two-photon peak also shows a Stark shift of up to 35 MHz and a power dependent increase in the spectroscopic width of the resonance.

To model this behavior, a master equation simulation involving three transmon levels and 50 cavity levels was employed. The model is quite sensitive to the coupler power which is incorporated through both cavity and qubit drive Rabi frequencies (Ω_r and Ω_q). Since these parameters are not well-known at the frequency $(\omega_q + \omega_r - \chi)/2$, we allow them to be free parameters in our master equation simulations. For this device $\Omega_r/\Omega_q = 6.3$ yields good agreement between simulations and experiments (Fig. 2). This ratio also agrees well with the predicted value based on our values for g , ω_r and ω_c [28].

The effective two-photon Rabi rate Ω_c , the ac-Stark shift, and the amount of population inversion all depend on the coupler drive power P_c . Obtaining the effective Rabi rate is non-trivial because the coupler drive between $|g0\rangle$ and $|e1\rangle$ can induce two-photon transitions between the levels via two paths: one via the intermediary state

$|e0\rangle$ and the other via $|g1\rangle$. If the levels were harmonic, these two paths would cancel out making the net transition rate zero [29]. Instead, the effective Rabi pumping rate [30] from $|g0\rangle$ to $|e1\rangle$ is given to lowest order by [31]

$$\Omega_c \simeq \frac{4\Omega_q\Omega_r\chi}{\Delta^2}. \quad (3)$$

To achieve coherent population trapping in our experiment, the coupler drive power was set so that $\Omega_c/2\pi = 874$ kHz.

Figure 2(b) shows a plot of the measured Stark shifted two-photon $|g0\rangle \leftrightarrow |e1\rangle$ resonance frequency versus Ω_q^2 . The resonant frequency was extracted at each value of Ω_q^2 by fitting the data in Fig. 2(a) to a Lorentzian. For comparison, the dashed red curve in Fig. 2(b) shows the theoretically expected Stark shift which is proportional to the anharmonicity in the system and is given to lowest order by [31, 32],

$$\frac{\Delta\omega_{|g0\rangle \rightarrow |e1\rangle}}{2} \simeq -\frac{1}{\Delta^2} \left(\frac{E_C\Omega_q^2}{\hbar} + \chi\Omega_r^2 \right). \quad (4)$$

Here, the first term is proportional to $E_C/h = 200$ MHz, which is the charging energy of the transmon and sets its anharmonicity. The solid blue line in Fig. 2 shows the results extracted from the master equation simulation shown in the inset to Fig. 2(a). Excellent agreement is obtained between the data, simulations and the theoretical model.

Fig. 2(c) shows a plot of the maximum excited state population $\mathcal{P}_e = 1 - \mathcal{P}_g$ versus effective coupler drive strength Ω_c . The data and simulations are in good agreement except for coupler powers $P_c > -91$ dBm where $\mathcal{P}_e \approx 0.94$ and $\Omega_c/2\pi = 874$ kHz. Above this power, the simulations suggest that the population begins to enter into the $|f\rangle$ state of the qubit. Furthermore, the fidelity did not improve above this coupler power (see Sec. IV).

B. Coherent Population Trapping and System Characterization

With the population inverted to $\mathcal{P}_e \approx 0.94$, using the continuous coupler tone at $P_c = -91$ dBm and $\Omega_c/2\pi = 874$ kHz, an arbitrary dark state $|D\rangle$ of our Λ -system was generated by illuminating the device with an additional tone at the transition frequency $|e0\rangle \leftrightarrow |e1\rangle$ at $\omega_p/2\pi = 7.94164$ GHz. By changing the drive strength Ω_p , we were able to change Θ of the dark state (see Eq. 1). Analysis of this behavior allowed us to determine some key system parameters.

Figure 3(a) shows a false color plot of the measured population \mathcal{P}_e versus coupler detuning Δ_c and probe power P_p . With the probe power off, a Lorentzian-like peak is observed with a width determined by κ and Ω_c (Fig. 3(b)). Above a probe power of -167 dBm a narrow spectroscopic dip is observed at $\Delta_c \simeq 0$ (Fig. 3(c)), indicative of an interference effect. As the probe power

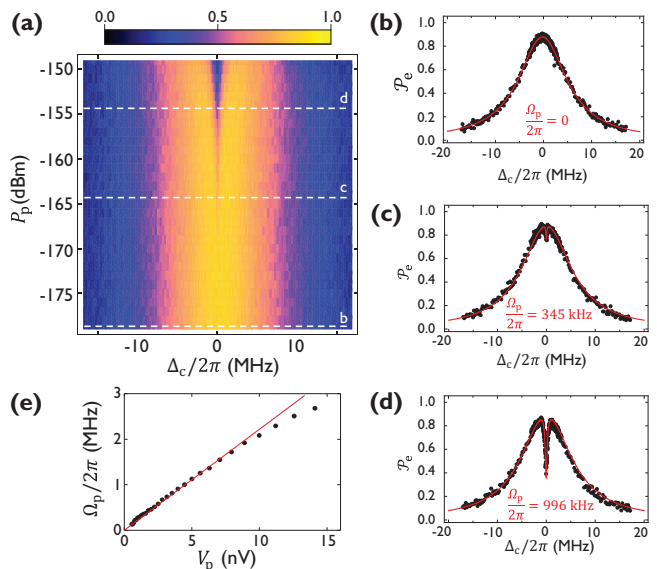


FIG. 3. (Color online) **Coherent population trapping spectroscopy.** (a) False color plot of \mathcal{P}_e for the coupler transition ($|g0\rangle \rightarrow |e1\rangle$) detuning Δ_c versus power P_p of the probe drive ($|e0\rangle \rightarrow |e1\rangle$). Linecuts of spectroscopy data (black dots) at probe powers (b) -179 dBm, (c) -164 dBm, and (d) -154 dBm along with theoretical fits (solid red) and fit values for Ω_p indicated. The probe-coupler detuning was set to $\delta/2\pi = 26$ kHz for all the curves. (e) Plot of extracted Ω_p versus applied probe voltage V_p allowed calibration of the probe strength. The linear fit (red line) gave $\Omega_p/2\pi = V_p \times 221.5$ kHz/nV.

increases, both the depth and the width of the dip increases (Fig. 3(d)).

The probe amplitude Ω_p was extracted by fitting each measured linecut of \mathcal{P}_e vs. Δ_c to a solution of the master equation for a driven three level system. The Λ -system was modeled with the Hamiltonian [8],

$$\mathcal{H}_{\text{tot}} = (\Delta_p - \Delta_c)|e0\rangle\langle e0| - \Delta_c|e1\rangle\langle e1| + \frac{1}{2}\Omega_c|e1\rangle\langle g0| + \frac{1}{2}\Omega_p e^{-i\phi}|e1\rangle\langle e0| + \text{h.c.} \quad (5)$$

where Δ_p and Δ_c are detunings as defined in Fig. 1(b). ϕ is the difference in initial phases of the coupler and probe drives when generated using the arbitrary waveform generator. The master equation was then found with decoherence effects included via Lindblad operators [33],

$$\begin{aligned} \frac{d\rho}{dt} = & \frac{i}{\hbar} [\rho, \mathcal{H}_{\text{tot}}] + \Gamma_1 \left(\mathcal{L}_q \rho \mathcal{L}_q^\dagger - \frac{1}{2} \{ \mathcal{L}_q^\dagger \mathcal{L}_q, \rho \} \right) \\ & + \kappa \left(\mathcal{L}_r \rho \mathcal{L}_r^\dagger - \frac{1}{2} \{ \mathcal{L}_r^\dagger \mathcal{L}_r, \rho \} \right) \\ & + \frac{\gamma}{2} \left(\mathcal{L}_{\text{dph}} \rho \mathcal{L}_{\text{dph}}^\dagger - \frac{1}{2} \{ \mathcal{L}_{\text{dph}}^\dagger \mathcal{L}_{\text{dph}}, \rho \} \right) \end{aligned} \quad (6)$$

where \mathcal{L}_q and \mathcal{L}_r are the decay operators for the qubit

and cavity respectively and \mathcal{L}_{dph} corresponds to the dephasing operator for the qubit.

Setting $d\rho/dt = 0$, the master equation (Eq. 6) was solved analytically in the steady state. The steady state population in $|e0\rangle$ was fit to the \mathcal{P}_e versus Δ_c dependence in Fig. 3(a). We first fit the spectroscopy of the $|g0\rangle \leftrightarrow |e1\rangle$ transition without the probe (Fig. 3(b)), with Ω_c and κ as free parameters. With Ω_c and κ then fixed, the rest of the spectroscopy data was fit with Ω_p and detuning δ as free parameters (Fig. 1(b)). The solid red curves in Fig. 3(c-d) show the results of these fits, along with the extracted probe amplitudes Ω_p . Note that for Fig. 3(d), $\Omega_p \approx \Omega_c$ which by Eq. 1 is the condition when $|D\rangle$ is in a symmetric coherent superposition of $|g0\rangle$ and $|e0\rangle$. Finally, Fig. 3(e) shows a plot of the extracted Ω_p versus the voltage amplitude of the drive, along with a fit to the expected linear dependence. The deviation of the data at high powers is likely due to the system being driven into states outside the three states in the Λ -system.

IV. CPT STATE TOMOGRAPHY

We next used quantum state tomography [20] to examine how well the system's dark state could be controlled in Θ and ϕ . We fixed the coupler amplitude at $\Omega_c/2\pi = 874$ kHz and set the frequency on resonance with the Stark shifted $|g0\rangle \leftrightarrow |e1\rangle$ transition such that $\Delta_c = 0$. The probe frequency was set to the $|e0\rangle \leftrightarrow |e1\rangle$ transition and the amplitude Ω_p was varied from 0 to 2 MHz, while the initial phase of the probe ϕ_p was varied over 360° in 5° steps. The initial phase of the coupler drive was held constant at 0.

The tomography data was acquired in the following manner. Both the coupler and the probe were applied continuously for a duration of 60 μs to allow the system to reach a steady state. These two tones were then turned off and state tomography was performed by either applying the identity (\mathbb{I}) or tomographic $\pi/2$ pulses around the X or Y axis of the Bloch sphere of the qubit, at $\omega_q/2\pi = 6.33121$ GHz. Each tomographic data point was averaged over 1000 shots before computing the Stokes parameters [20],

$$r_x = 2\mathcal{P}_Y - 1 \quad (7)$$

$$r_y = 2\mathcal{P}_X - 1 \quad (8)$$

$$r_z = 1 - 2\mathcal{P}_\mathbb{I}. \quad (9)$$

where $\mathcal{P}_\mathbb{I}$, \mathcal{P}_X and \mathcal{P}_Y are the measured outcome probabilities after performing the corresponding \mathbb{I} , X , or Y tomographic pulses immediately followed by a qubit population measurement in the σ_z basis. Figure 4(a) shows false color plots of the Stokes parameters when the tomography was performed at different probe powers Ω_p and different ϕ_p .

Figure 4(d) shows a plot of r_z as a function of ϕ_p for three different values of Ω_p . As Ω_p increases, we see that r_z increases from -0.87 up to $+0.65$. As expected,

the variation of r_z with ϕ_p is small, with a maximum deviation of 0.09. The azimuthal Stokes parameters, r_x and r_y (Fig. 4(b-c)) show clear sinusoidal patterns that are 90° out-of-phase with each other and the amplitude of oscillations are largest when $\Omega_p/2\pi = 947$ kHz. The point where $\Omega_p = \Omega_c$ coincides with when $r_z \simeq 0$. We note that varying the phase ϕ_c of the coupler tone results in doubling of the period for r_x and r_y which is a result of the coupler being a two photon process [31].

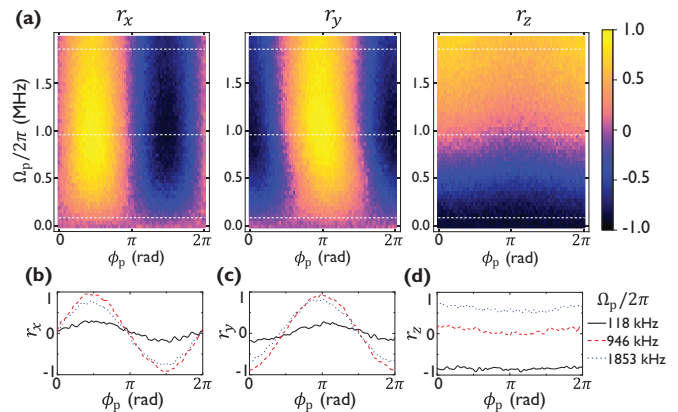


FIG. 4. (Color online) **Quantum state tomography of the trapped state vs. probe phase.** (a) False-color plots of r_x , r_y and r_z versus Ω_p and ϕ_p . (b) Linecut plots (along dashed lines in (a)) of Stokes parameters r_x , (c) r_y and (d) r_z versus ϕ_p at probe powers 118 kHz (solid black), 946 kHz (dashed red), and 1853 kHz (dotted blue).

For each Ω_p , the r_x and r_y versus ϕ_p data were independently fit to a sinusoidal function with amplitude r_\perp . Since a small variation in the z -component was observed versus ϕ_p , an average value for r_z was calculated. To quantify the accuracy of the phase control, we then found the root-mean-square deviation between the fits and data. If the entire deviation is attributed to the phase, we obtain an error of 6° for phase control. Figure 5(a-b) shows the analysis for r_z and r_\perp versus Ω_p . The r_z component starts at $r_z = -0.87$ at $\Omega_p = 0$ and monotonically increases towards the north pole of the Bloch sphere as Ω_p increases. On the other hand, r_\perp shows a maximum value of $r_\perp^{\text{max}} = 0.92$ where $r_z \approx 0$, before decreasing as Ω_p is increased. The red solid curves are the theoretical predictions with no free parameters.

The theoretical model used to generate the solid red curves in Fig. 5 only included the three levels $|g0\rangle$, $|e0\rangle$ and $|e1\rangle$. Furthermore, the coupler drive was modeled as an effective single-photon drive. Due to the high pump strengths used, some leakage to levels outside the Λ -system is inevitable. Although these factors will limit the fidelity of the process, the agreement obtained with the theory was satisfactory.

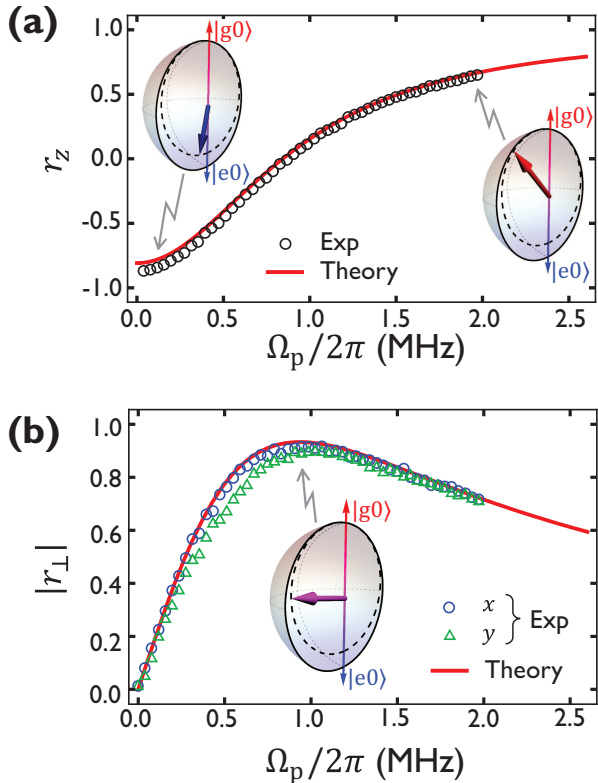


FIG. 5. (Color online) **Dark state tomography.** (a) Plot of r_z versus Ω_p . The data (black circles) is in good agreement with the theory (solid red curve). (b) Plot of $|r_\perp|$ versus Ω_p . The data from the x -variation (blue circles) and y -variation (green triangles) are compared with the theoretical prediction (solid red curve). Insets show the state of the system as points on the Bloch sphere for three values of Ω_p .

V. DISCUSSION AND CONCLUSIONS

In this experiment, we examined a cQED Λ -system created by coupling a transmon to a cavity with the relaxation rates engineered so that $\kappa \gg \Gamma_1$. Simultaneously driving the two-photon process $|g0\rangle \leftrightarrow |e1\rangle$ and the $|e0\rangle \leftrightarrow |e1\rangle$ transition allowed formation of a coherently

trapped dark state. The system parameters were extracted by performing two-photon spectroscopy and the dark state analyzed using quantum state tomography. By varying the phase and amplitude of the probe tone, coherent control of the dark state was demonstrated. A maximum population inversion of $\mathcal{P}_e = 94\%$ was obtained, while the fidelity for the generated maximal superposition state was $\mathcal{F} = 96\%$. The maximal root-mean-square error for phase control of superpositions was found to be 6° .

A small oscillation was observed in r_z when ϕ_p was varied, possibly due to an effective tilt in the axes during tomography. As the tomographic measurements were performed immediately following halting of the coupler and probe tones, the induced Stark shifts in the system may have affected the results. An interesting comparison would be to observe r_z after turning off the coupler and probe tones adiabatically, on a timescale much longer relative to the expected Stark shift.

In principle, further improvements in the fidelity of the dark state can be achieved by increasing the anharmonicity of the transmon which can be obtained by increasing the ratio $E_C/\hbar\omega_q$. This would reduce leakage to the $|f\rangle$ state at high Ω_c . Further improvements could be obtained by increasing the ratio κ/Γ_1 . Although this could be accomplished by increasing the lifetime of the qubit, we are currently limited by the Purcell effect [34]. Finally, pumping the system using two different coupler tones, rather than a single coupler drive, may further increase the process fidelity. With two tones it will be possible to decrease the detuning between the drives and the intermediate state, and this would allow stronger two-photon drives for the coupler transition [24, 30, 35].

ACKNOWLEDGMENTS

The authors thank S. Novikov and T. Sweeney for insightful discussions. F.C.W. acknowledges support from the Joint Quantum Institute and the Center for Nanophysics and Advanced Materials.

-
- [1] H. R. Gray, R. M. Whitley, and C. R. Stroud, *Opt. Lett.* **3**, 218 (1978).
 [2] D. F. Phillips, A. Fleischhauer, A. Mair, R. L. Walsworth, and M. D. Lukin, *Phys. Rev. Lett.* **86**, 783 (2001).
 [3] N. S. Ginsberg, S. R. Garner, and L. V. Hau, *Nature* **445**, 623 (2007).
 [4] E. Arimondo and G. Orriols, *Lettere al Nuovo Cimento* **17**, 333 (1976).
 [5] E. Arimondo, “Coherent population trapping in laser spectroscopy,” in *Progress in Optics*, Vol. 35, edited by E. Wolf (Elsevier, Amsterdam, 1996) pp. 257–354.
 [6] M. Fleischhauer, A. Imamoglu, and J. P. Marangos, *Rev. Mod. Phys.* **77**, 633 (2005).
 [7] C. G. Yale, B. B. Buckley, D. J. Christle, G. Burkard, F. J. Heremans, L. C. Bassett, and D. D. Awschalom, *Proc. Natl. Acad. Sci.* **110**, 7595 (2013).
 [8] S. Novikov, T. Sweeney, J. E. Robinson, S. P. Premaratne, B. Suri, F. C. Wellstood, and B. S. Palmer, *Nat. Phys.* **12**, 75 (2016).
 [9] A. Blais, R.-S. Huang, A. Wallraff, S. M. Girvin, and R. J. Schoelkopf, *Phys. Rev. A* **69**, 062320 (2004).
 [10] A. Wallraff, D. I. Schuster, A. Blais, L. Frunzio, R.-S. Huang, J. Majer, S. Kumar, S. M. Girvin, and R. J. Schoelkopf, *Nature* **431**, 162 (2004).

- [11] T. Y. Abi-Salloum, *Phys. Rev. A* **81**, 053836 (2010).
- [12] J. F. Poyatos, J. I. Cirac, and P. Zoller, *Phys. Rev. Lett.* **77**, 4728 (1996).
- [13] D. Marcos, A. Tomadin, S. Diehl, and P. Rabl, *New J. Phys.* **14**, 055005 (2012).
- [14] K. W. Murch, U. Vool, D. Zhou, S. J. Weber, S. M. Girvin, and I. Siddiqi, *Phys. Rev. Lett.* **109**, 183602 (2012).
- [15] U. Vool, S. Shankar, S. O. Mundhada, N. Ofek, A. Narla, K. Sliwa, E. Zaly-Geller, Y. Liu, L. Frunzio, R. J. Schoelkopf, S. M. Girvin, and M. H. Devoret, *Phys. Rev. Lett.* **117**, 133601 (2016).
- [16] M. E. Kimchi-Schwartz, L. Martin, E. Flurin, C. Aron, M. Kulkarni, H. E. Tureci, and I. Siddiqi, *Phys. Rev. Lett.* **116**, 240503 (2016).
- [17] K. Geerlings, Z. Leghtas, I. M. Pop, S. Shankar, L. Frunzio, R. J. Schoelkopf, M. Mirrahimi, and M. H. Devoret, *Phys. Rev. Lett.* **110**, 120501 (2013).
- [18] J. D. Teufel, T. Donner, D. Li, J. W. Harlow, M. S. Allman, K. Cicak, A. J. Sirois, J. D. Whittaker, K. W. Lehnert, and R. W. Simmonds, *Nature* **475**, 359 (2011).
- [19] J. Chan, T. P. M. Alegre, A. H. Safavi-Naeini, J. T. Hill, A. Krause, S. Groblacher, M. Aspelmeyer, and O. Painter, *Nature* **478**, 89 (2011).
- [20] Y.-x. Liu, L. F. Wei, and F. Nori, *Phys. Rev. B* **72**, 014547 (2005).
- [21] J. Koch, T. M. Yu, J. Gambetta, A. A. Houck, D. I. Schuster, J. Majer, A. Blais, M. H. Devoret, S. M. Girvin, and R. J. Schoelkopf, *Phys. Rev. A* **76**, 042319 (2007).
- [22] H. Paik, D. I. Schuster, L. S. Bishop, G. Kirchmair, G. Catelani, A. P. Sears, B. R. Johnson, M. J. Reagor, L. Frunzio, L. I. Glazman, S. M. Girvin, M. H. Devoret, and R. J. Schoelkopf, *Phys. Rev. Lett.* **107**, 240501 (2011).
- [23] E. T. Jaynes and F. W. Cummings, *Proc. IEEE* **51**, 89 (1963).
- [24] A. Wallraff, D. I. Schuster, A. Blais, J. M. Gambetta, J. Schreier, L. Frunzio, M. H. Devoret, S. M. Girvin, and R. J. Schoelkopf, *Phys. Rev. Lett.* **99**, 050501 (2007).
- [25] P. J. Leek, S. Filipp, P. Maurer, M. Baur, R. Bianchetti, J. M. Fink, M. Göppl, L. Steffen, and A. Wallraff, *Phys. Rev. B* **79**, 180511 (2009).
- [26] W. F. Kindel, M. D. Schroer, and K. W. Lehnert, *Phys. Rev. A* **93**, 033817 (2016).
- [27] M. D. Reed, L. DiCarlo, B. R. Johnson, L. Sun, D. I. Schuster, L. Frunzio, and R. J. Schoelkopf, *Phys. Rev. Lett.* **105**, 173601 (2010).
- [28] L. S. Bishop, *Circuit Quantum Electrodynamics*, Ph.D. thesis, Yale University (2010).
- [29] C. Cohen-Tannoudji, J. Dupont-Roc, and G. Grynberg, *Atom-Photon Interactions* (John Wiley & Sons, Inc., 1998) pp. 207–210.
- [30] P. G. Di Stefano, E. Paladino, T. J. Pope, and G. Falci, *Phys. Rev. A* **93**, 051801 (2016).
- [31] See Supplemental Material at [URL will be inserted by publisher] for derivation of coupler drive properties and details on the readout method.
- [32] J. Bakos, *Physics Reports* **31**, 209 (1977).
- [33] G. Lindblad, *Comm. Math. Phys.* **48**, 119 (1976).
- [34] A. A. Houck, J. A. Schreier, B. R. Johnson, J. M. Chow, J. Koch, J. M. Gambetta, D. I. Schuster, L. Frunzio, M. H. Devoret, S. M. Girvin, and R. J. Schoelkopf, *Phys. Rev. Lett.* **101**, 080502 (2008).
- [35] M. Weissbluth, *Photon-Atom Interactions* (Academic Press, Inc., 1989) pp. 370–376.